J MATER RES TECHNOL. 2020;9(xx):13825–13841

Available online at www.sciencedirect.com

jmr&t Journal of Materials Research and Technology

https://www.journals.elsevier.com/journal-of-materials-research-and-technology

Original Article

The role of collagen in the dermal armor of the boxfish

Sean N. Garner[a,*], *Steven E. Naleway*[b], *Maryam S. Hosseini*[c], *Claire Acevedo*[b], *Bernd Gludovatz*[d], *Eric Schaible*[e], *Jae-Young Jung*[a], *Robert O. Ritchie*[e], *Pablo Zavattieri*[c], *Joanna McKittrick*[f]

[a] *Materials Science and Engineering Program, University of California, San Diego, La Jolla, CA 92093–0411, USA*
[b] *Department of Mechanical Engineering, University of Utah, Salt Lake City, UT 84112, USA*
[c] *Lyles School of Civil Engineering, Purdue University, West Lafayette, IN 47907, USA*
[d] *School of Mechanical & Manufacturing Engineering, UNSW Sydney, NSW 2052, Australia*
[e] *Advanced Light Source, Lawrence Berkeley National Laboratory, Berkeley, CA 94720, USA*
[f] *Department of Mechanical and Aerospace Engineering, University of California, San Diego, La Jolla, CA 92093–0411, USA*

ARTICLE INFO

Article history:
Received 1 June 2020
Accepted 24 September 2020
Available online 5 October 2020

Keywords:
Boxfish
Bouligand structure
Honeycomb structure
Finite element analysis *in situ*
small-angle x-ray scattering

ABSTRACT

This research aims to further the understanding of the structure and mechanical properties of the dermal armor of the boxfish (*Lactoria cornuta*). Structural differences between collagen regions underlying the hexagonal scutes were observed with confocal microscopy and microcomputed tomography (μ-CT). μ-CT revealed a tapering of the mineral plate from the center of the scute to the interface between scutes, suggesting the structure allows for more flexibility at the interface. High-resolution μ-CT revealed, for the first time, a 3D image of the dermal armor's complex collagen structure. Helical interfibrillar gaps in the collagen base were found that are similar to the Bouligand-type structure of the lobster, *Homarus americanus*, thereby suggesting that the collagen in the boxfish is also of a Bouligand-type structure. *In situ* scanning electron microscopy tests were performed in shear and tension between two connected scutes and suggest that the interfacial collagen is structurally designed to preferentially absorb energy during deformation to protect the internal collagen. Similarly, *in situ* small-angle x-ray scattering was performed in shear and tension and further corroborated the complex collagen structure. Lastly, these experimental results are coupled with finite element simulations that characterize the interfacial collagen and corroborate the non-linear deformation response seen during *in situ* testing. Overall, these findings further the understanding of the structure and mechanics of the dermal armor of the boxfish which may help provide a basis to synthesize bioinspired composites for impact-resistant materials, specifically with bioinspired Bouligand-type structures to create novel fiber-reinforced composites.

* *Corresponding author.*
E-mails: sean.n.garner@gmail.com, sgarner@eng.ucsd.edu (S.N. Garner).
https://doi.org/10.1016/j.jmrt.2020.09.090

1. Introduction

Overlapping scale patterns are common amongst marine and freshwater fish species. These overlapping structures have developed as full coverage of the fish's body which simultaneously provide protection from predators while maintaining flexibility for swimming and other body motions [1]. There are, however, a small number of fish species that employ more rigid armor. Many of the species in the *Ostraciidae* family use rigid armor in their defense [2,3]. Recent work by Yang et al. [4] provided insight into the armor of the boxfish, but also provided for a number of additional questions into this alternative armor style.

The scales and scutes of fish species are capable of providing effective protection from predation through a layered, composite structure [5–8]. This structure tends to consist of a highly mineralized surface plate (often made of bony or enamel-like materials) and a less-mineralized, collagen base [6,7,9–12]. The less mineralized collagen base is most often formed in a twisted plywood, or Bouligand structure [13–15], which consists of planes of aligned collagen fibrils stacked on top of each other with each layer slightly rotated [1]. The Bouligand structure also appears in several other impact resistant biological materials including the exoskeletons of arthropods and the dactyl club of the mantis shrimp [16–18]. The reason for its universality within biopolymer composites in the natural world is due to its optimization of several parameters including (1) creating quasi-isotropic fiber reinforced materials to avoid weakness in a given axis; (2) allowing for the fibers to reorient along the loading axis to provide more resistance [13]; (3) improving energy dissipation and stress relaxation by influencing cracks to follow the helical fiber orientations thereby maximizing crack surface area per unit volume [19].

When attacked by a predator, the layered structure of fish scales and scutes provides both protection from the sharp piercing action of a tooth (through the hardened surface plate) and the powerful compressive and crushing force of the jaws (through the tough collagen base) [7]. Beyond the functions of an individual scale, the overlapping structure of scales can provide protection. Vernerey and Barthelat [20–22] analytically studied these structures in fish and showed that, by balancing the scale length and spacing between scales with the total body length, many species are capable of large overall body flexibility, while minimizing the rotation of individual scales, thus resisting puncture when attacked. While this overall body flexibility is important for motion, it also plays a significant role in defense. In addition, the flexibility of the body itself provides some energy absorbance as the piercing tooth of a predator will cause the body to deform and the overlapping scales to lock together before stress is directly applied to the scale [22]. Due to this success, overlapping scale structures are found in a variety of animals including most teleost fish [7,9,11,12,23], pangolin [24], and chiton [25], and has led to a number of bioinspired armor designs [8,26]. Given these benefits of overlapping structures, a fish species that employs rigid armor would be unwise to forsake all flexibility.

In this study, the dermal armor of the longhorn cowfish (*Lactoria cornuta*, Fig. 1), a type of boxfish, is structurally and mechanically characterized. Fig. 2 shows a diagram of the features of the boxfish's armor, similar to those previously reported [3,4]. The rigid armor consists of non-overlapping, primarily hexagonal scutes (Fig. 2a) [4]. Similar to many other fish scales, the scutes themselves are made of hydroxyapatite mineral and type I collagen and are structured as a highly mineralized surface plate (1:0.33 mineral-to-collagen ratio) sitting on a collagen base (1:12 mineral-to-collagen ratio) [4]. The mineralized surface plate features raised ridges that extend from the center of the scute to the edges. The interface between scutes is made of interlocking mineralized triangular sutures, which are unlike many similar structures in nature as they are devoid of any bridging Sharpey's fibers or compliant phase (Fig. 2b) [4]. Geometric analysis of triangular sutured structures by Li et al. [27–29] demonstrated that the teeth angles of the boxfish's sutures ($2\theta = 50.6^{\circ}$) were considerably different from what would be expected to maximize the strength of the interface ($2\theta = 23.6^{\circ}$). This contrast between the theoretical optimized angle for strength in sutured interfaces and actual angle of suture teeth in the boxfish is likely due to the former being calculated while including a compliant phase junction between sutured interfaces that is not found in the boxfish sutures. Additionally, these results may also suggest that boxfish suture's geometry are not solely optimized for strength [4].

Fig. 1 – Lateral view of the boxfish (*Lactoria Cornuta*), commonly referred to as the longhorn cowfish. Image taken from [33].

The collagen base itself, imaged with scanning electron microscopy (SEM), revealed two important features illustrated in Fig. 2c [4]. First, the interior of the scute consists of periodic patterns in the collagen structure, similar to the Bouligand structure found in the scales of most fish species, but different in terms of the orientation of the periodic axis with respect to the thickness of the dermis. Typically, Bouligand structures found in nature align the periodic axis with the primary loading directions, as seen in the collagen phase underneath the mineral plates in teleost fish scales [13,18]. However, as shown in Fig. 2c the direction of the periodic axis changes from being orthogonal to the mineral plate near the distal and lateral regions (where 'distal' refers to the anatomically outer regions of boxfish dermis where the mineral plate is, and 'lateral' refers to the peripheral edges of the hexagonal scute) to being parallel, like its teleost counterparts, near the proximal and central regions. This unique structure has prompted us to further investigate the local structure of the collagen fibrils in this underlying network and determine if it is a ladder-like structure, as previously claimed [4].

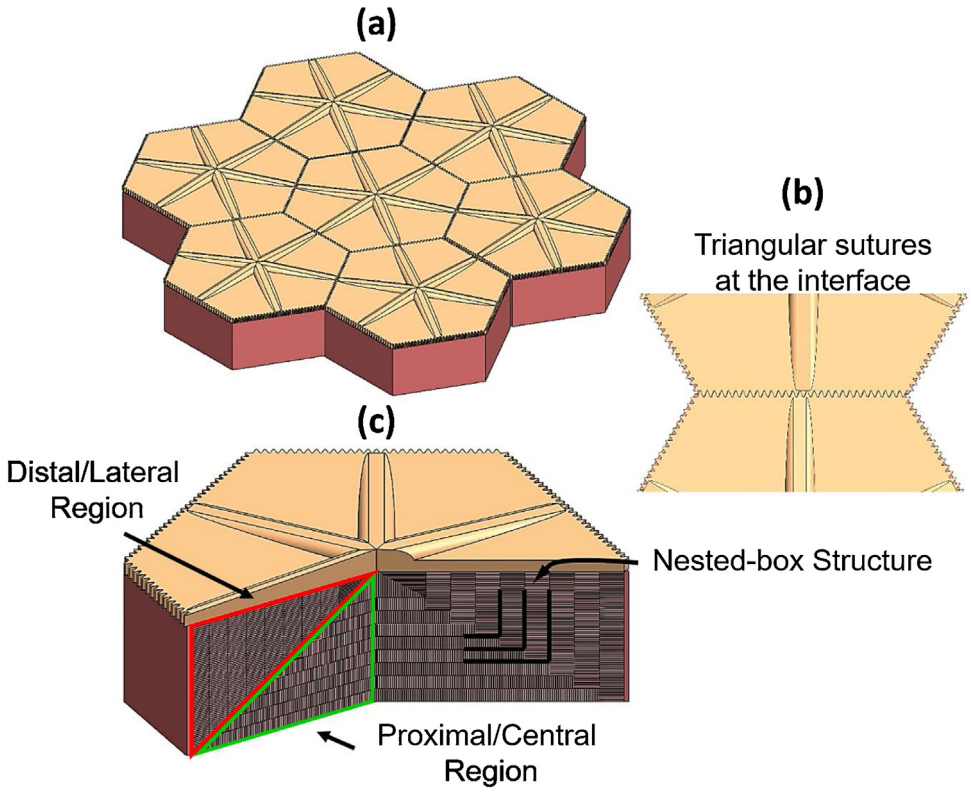

Fig. 2 – Boxfish armor structure, as previously reported [4]. (a) The armor consists of predominately hexagonal scutes that feature raised ridges extending from their center to edge; (b) The scutes do not overlap, but instead have interlocking suture structures at their interfaces; (c) The scutes consist of a mineralized surface plate and a collagen base. The base is complex, consisting of interlaid collagen frames that feature ladder-like collagen structures that are organized into an overall nested-box structure. The nested-box structure contains two distinct regions (distal/lateral and proximal/central) where the axes of periodicity are orthogonal to one another.

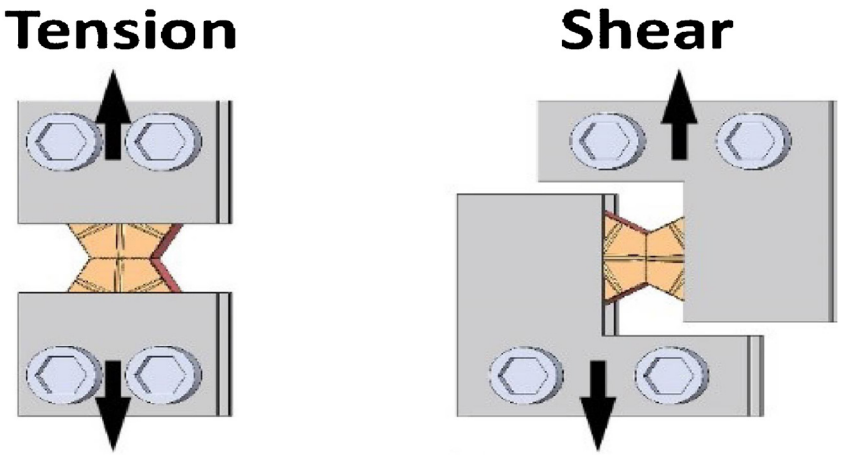

Fig. 3 – Schematic diagram of mechanical fixtures employed for *in situ* mechanical tests (with scanning electron microscopy and small-angle x-ray scattering) in both tensile and shearing modes.

In this work we build upon previous knowledge and present new evidence of the mechanisms that allow the boxfish to maintain flexibility and protection despite its rigid armor. The rigid dermal armor enables the boxfish to survive in its natural environment despite the lack of speed and ability to undulate like most other fish. Understanding the boxfish's dermal armor and specifically the complex collagen network beneath the mineralized scutes, will aid in future bioinspired engineering pursuits. For example, novel materials have been synthesized inspired by the Bouligand structure that range from additive manufacturing resilient ceramic-polymer composites, self-assembling cellulose nanocrystals

into a Bouligand structure to create a tough and strong photonic film, and also bio-templating a Bouligand structure from crustacean shells to create a hydrogel that changes color based on pH [30–32]. Essentially, utilizing this naturally ubiquitous structure in bioinspired engineering endeavors is creating novel fibrous composites with a combination of efficient mechanical performance and photonic properties. Therefore, further exploration and study of unique analogs of Bouligand-type structures found in nature can add to the repertoire for future bioinspired engineering.

2. Materials and methods

Two boxfish samples were obtained from the Scripps Institution of Oceanography at the University of California, San Diego (*Lactoria cornuta,* catalog numbers SIO 14-20, SIO 95-125, SIO 95-141). A representative image [33] is shown in Fig. 1. Samples were preserved in a 1:1 isopropanol and water solution to induce a semi-dehydrated state. The two fish selected measured ~50 mm in length and ~100 mm in length.

2.1. Structural characterization

Scutes were cut from the mid-section of the boxfish samples using a scalpel such that each specimen consisted of two neighboring, connected, hexagonal scutes. Imaging was performed on 15 dehydrated specimens with the mineralized plates carefully polished to reveal the underlying collagen base. Polishing was carried out with 1700-grit SiC paper, using water as a lubricant, prior to sonicating in water to remove residuals. Scanning electron microscopy (SEM) was performed on 14 of these pairs of scutes. Another pair was infiltrated with OsO_4, critically point dried, fixed in epoxy, and polished to a shine such that the collagen surfaces could be better observed. This pair of polished and stained scutes was used in both three-dimensional (3D) imaging with micro-computed tomography (μ-CT) and with confocal microscopy (Keyence VH-Z100UR).

Both the low- and high-resolution μ-CT was performed using a Zeiss Versa 510 microscope with a voxel size of 9 μm and 535 nm, respectively. The resulting μ-CT images (2401 projections) were edited and stitched together using the Amira software (Thermo Fisher Scientific, Waltham, Massachusetts) to create a high-resolution 3D image.

2.2. In situ mechanical characterization

2.2.1. In-situ scanning electron microscopy

The scutes were mechanically analyzed using *in situ* tests within the SEM. Prior to testing, all samples were rehydrated in Hanks' balanced salt solution for 24 h, then immediately tested, to ensure that all tests were performed in a hydrated state. To understand the rigid, non-overlapping interfaces of the boxfish's armor, the scute samples were tested in tension and shearing loading modes (see Fig. 3a) with a focus on the interface between scutes. To ensure this, the samples were carefully sectioned with a scalpel from the boxfish to include exactly two scutes with a single, unaltered interface between them. In addition, samples were tested both in an intact form and with the surface mineralized plate removed. The surface plate was carefully polished off using same method mentioned in Section 2.1.

In situ SEM testing was performed under step-loading at a displacement rate of 0.1 mm/min (slowest displacement rate available to best observe deformation mechanisms of collagen structures) using a Gatan Microtest 2 kN bending stage (Gatan, Abington, UK) in a S4300SE/N variable pressure SEM (Hitachi America, Pleasanton, CA, USA) operated at a partial pressure of 35 Pa. Five samples were tested with the mineralized plate intact and seven were tested with the mineralized plate removed.

2.2.2. In situ small-angle x-ray scattering

Small-angle x-ray scattering (SAXS) patterns were collected during *in situ* uniaxial tensile testing at beamline 7.3.3 at the Advanced Light Source x-ray synchrotron at the Lawrence Berkeley National Laboratory [34]. As each scute was put under load, simultaneous measurements were made of the deformation of the tissue on the macro scale, as well as the deformation of the collagen fibrils within the tissue on the nanoscale.

Scutes were prepared for such SAXS analysis, as described above for *in situ* SEM testing. The scutes were clamped at their extremities into the jaws of TST-350 tensile stage (Linkam Scientific, Inc.) and subjected to a displacement rate of 5 μm/s. Five of the scutes were measured in tension, and three in shear. During testing, each sample was exposed to x-rays of 10 keV energy for 1 s every 7.5 s, with the changing x-ray scattering patterns collected with a Pilatus3 2 M detector (Dectris, Ltd.) at a distance of approximately 4 m. The cumulative irradiation dose was kept underneath the limit of 30 kGy in order to minimize irradiation damage to the tissue which could affect its mechanical behavior [35]. Given these irradiation conditions, the displacement rate was chosen to be quick enough to prevent damaging irradiation of sample. Although hydration and drying of the sample in air was a concern, the power of the beam was considered too weak (on the order of a milliwatt) to cause significant heating. Therefore, hydration was not monitored.

Scattering of the x-rays, specifically with the *d*-period of the collagen fibrils, a 67 nm regular pattern of molecular gaps and overlaps, acted to create Bragg peaks on the detector, and as this molecular pattern was stretched by the applied loads, the strain in the fibrils could be measured from the resulting shifts in the Bragg peaks., *i.e.*, the *d*-period of the collagen fibrils was used an a nanoscale strain gauge. The SAXS data were analyzed with custom software written in LabVIEW, which subtracted out the background intensity with spline fits, located the azimuthal center of each Bragg peak with a Gaussian fit, and made a 5-degree radial integration around each azimuthal center. The *d*-period of the collagen fibrils was measured by fitting this radial integration with an exponentially modified Gaussian. The fibril strain was then derived from the changes in *d*-period, as compared to the *d*-period at zero load. The SAXS patterns also contained broader dot-shaped peaks created by the interaction of the x-rays with the regular lateral packing of the collagen fibrils; these were analyzed using the same software.

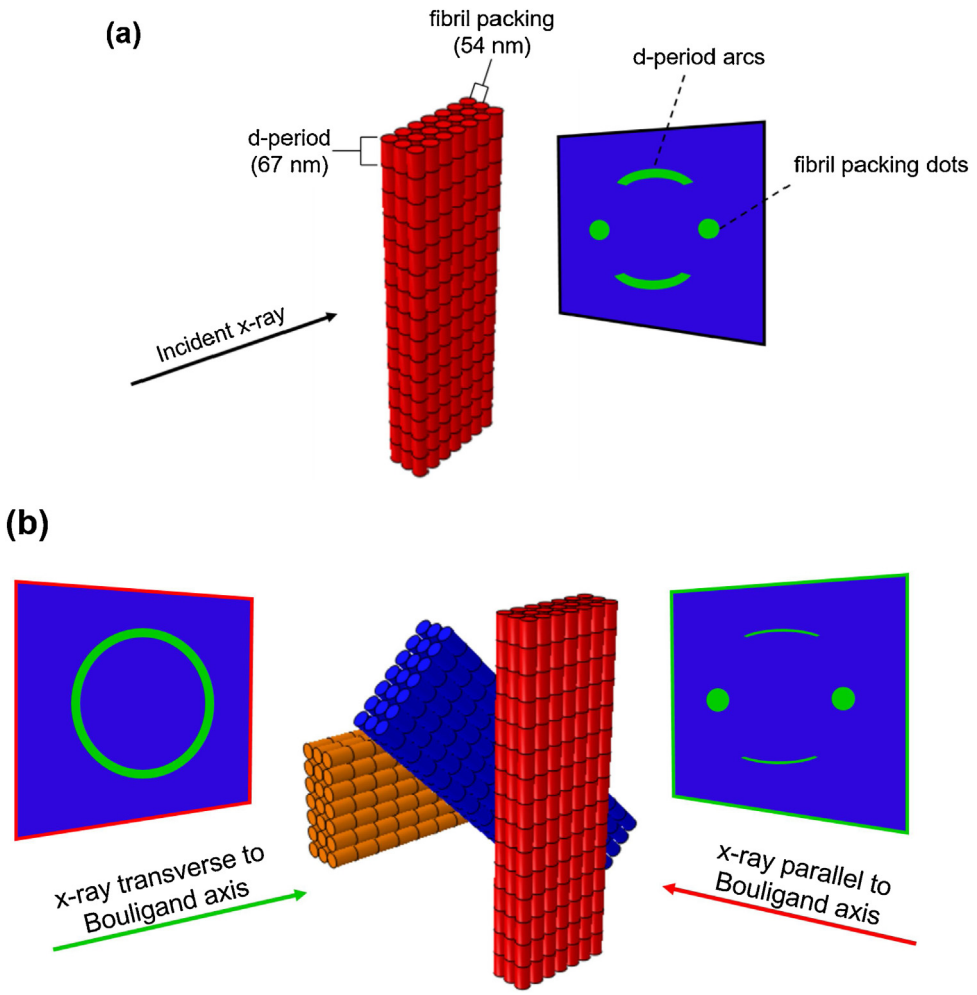

Fig. 4 – (a) Small-angle x-ray scattering diffraction pattern from analyzing a unidirectional network of packed collagen fibrils that are orthogonal to the incident x-rays. The periodicity of the characteristic *d*-period in collagen fibril as well as the packing of the fibrils are observed in the diffraction pattern which are represented by the arcs and dots, respectively. (b) Diffraction pattern from analyzing a rotating network of packed collagen fibrils (*i.e.*, Bouligand structure). When the incident x-rays are transverse to the axis of rotation (*i.e.*, Bouligand axis) a diffraction pattern that is nearly identical to the unidirectional network of fibrils, (a), however, the ratio of the intensity of the *d*-period arcs and lateral packing dots should be less due to the *d*-period of the fibrils becoming hidden to the incident x-rays as the lamellae rotate to become parallel with x-ray path. The lateral packing of fibrils should be observed regardless of the angle of rotation of the lamellae. When the Bouligand structure is analyzed parallel to the Bouligand axis, a concentric ring is observed if the angle of rotation between lamellae is small enough due to overlap between *d*-period arcs and lateral packing dots that represent each lamella.

The tissue strain was obtained by collecting visible light charge coupled device (CCD) images of the scutes in parallel with the x-ray scattering data. The CCD images were processed with digital image correlation methods to follow the changes in spacing of patterns on the outside surface of the scute.

Previous reports on the use of SAXS on the collagen structures in fish scales have shown a diffraction pattern with distinct concentric arcs, corresponding to the *d*-period of the collagen fibril and its harmonics [13]. Fig. 4a shows a diagram of this, where the lateral packing distance between collagen fibrils is displayed in the enlarged dots (horizontally aligned dots) and *d*-period spacing within collagen fibrils orthogonal to the x-ray beam are displayed in the smaller arcs (vertically aligned arcs). These characteristic x-ray interactions with complex collagen systems have also been well-documented in research performed in the past few decades with SAXS on human cornea collagen structures [36]. Fig. 4b illustrates a simplified Bouligand structure (with only 0-45-90° oriented lamellae) where the diffraction patterns are expected from performing SAXS either transverse or parallel to the Bouligand (or helical) axis. It is important to note that Bouligand structures in biological materials typically have significantly smaller rotations between lamellae which give rise to overlapping arcs/dots which form a continuous circle for the diffraction pattern, as opposed to a few discrete arcs [11]. Furthermore, by comparing Fig. 4a with b, the diffraction patterns for a unidirectional system can be seen to have a similar pat-

tern produced from the Bouligand structure transverse to its helical axis. This occurs because collagen fibrils are orthogonal (in red) to the incident x-rays (as in the unidirectional network); however, as the lamellae rotate to become parallel with x-ray (in orange) the *d*-period of these layers becomes effectively hidden to the incident x-ray while the lateral packing of the fibrils remains. Therefore, the key difference between these two diffraction patterns is that the ratio of intensities between the *d*-period arcs and lateral packing dots will be less in the case of the Bouligand structure which allows for a nuanced strategy to tell the two structures apart.

3. Results and discussion

3.1. *Confocal microscopy*

Confocal microscopy provided a relatively quick and easy approach to observe the underlying collagen structure within a boxfish scute to provide a basis for further advanced imaging. Fig. 5a reveals a cross-section of the scute collagen network where it is clear that there is a periodic structure present that changes its axis of periodicity throughout the scute, giving rise to the nested-box structure previously observed [3]. Moreover, Fig. 5a reveals that the pitch length (180° rotation of collagen planes) of the proximal/central of the nested-box decreases (~ 5 times smaller) compared to the distal/lateral regions.

Fig. 5b provides a closer look at the interface between two scutes and reveals there seems to be a difference in contrast between the inner collagen (nested-box) and the interfacial collagen. This difference suggests there is a structural difference between the two types of collagen that is further explored using μ-CT, SEM and subsequently SAXS. A top-down view of a scute with its mineral plate carefully polished off, in Fig. 5c, reveals that the periodic structure aligns itself with the scutes' hexagonal edges. Artifacts of damage from polishing can also be seen.

3.2. *Micro-computed tomography*

High-resolution μ-CT was performed to determine the organization of collagen fibrils in the periodic regions. These 3D images revealed the helical interfibrillar gaps (seen as blue parallel lines in Fig. 6b) that are similar to those in the twisted plywood, or Bouligand-type, structure of the exoskeleton of the lobster *Homarus americanus* and cuticle of the weevil *Curculio longinasus* [37–39]. This evidence corroborates research done by Besseau and Bouligand [3] to characterize the twisted plywood (Bouligand-type) structure in the collagen structure of the boxfish. However, this structure is contradictory to the most recent work by Yang et al. [4] that hypothesized the collagen structure in the boxfish scute follows a ladder-like structure rather than a Bouligand-type structure, *i.e.*, that the periodic structure seen on the top surface consists of rows of collagen planes separated and connected by orthogonal planes acting as the rungs of the 'ladder'. These claims, although proven here to be incorrect, still demonstrate that this structure consists of a unique type of Bouligand-type arrangement that can be confused for a different structure (ladder-like) when observing only the surface. Fig. 6 reveals, using 3D imaging, the apparent rungs of the ladder-like structure are in-fact the tips of the helical interfibrillar gaps being exposed. The helical gaps are exposed on the top face when the long axis of the gaps are parallel to the thickness of the dermis and on the front face when the width is orthogonal to the thickness. Although the Bouligand-type structure was revealed through the imaging of the helical interfibrillar gaps in the distal/lateral regions of the nested-box structure (Fig. 6), these gaps did not appear in the proximal/central regions where the axis of periodicity changes to become parallel with the dermis. The absence of observable gaps and a decrease in pitch length previously suggested from confocal microscopy suggests this region maintains less ductility and more stiffness than the top/side regions.

The boxfish employs a complex and hierarchical network of collagen beneath its unique hexagonal scutes that we are now beginning to understand. The Bouligand structure, observed in many impact resistant natural materials manifests itself in varying materials (*i.e.*, collagen and chitin) and length scales (*e.g.*, the pitch length can vary from ~220 nm in *Cotinis mutabilis* exocuticle to 100 μm in the dactyl club of the mantis shrimp) [17,18]. Moreover, the Bouligand structure found in the lobster exoskeleton possesses a unique type of honeycomb structure that is a variant of the Bouligand structure with interfibrillar gaps dispersed throughout the helical collagen fibrils that are proposed to act as microchannels for nutrient transport and also resist fiber pullout [37,38]. In this study, using μ-CT, it was observed that the distal/lateral regions of the collagen layer of the scute employs this honeycomb structure of helical interfibrillar gaps. Although this type of honeycomb structure has been observed before, the boxfish appears to uniquely utilize an abrupt shift in the helical axis giving rise to the previously described nested-box structure. Typically, for Bouligand structures found in natural materials, the helical axis aligns with the loading/impact axis (*e.g.*, fish scale's helical axis aligns with the thickness of the scale) [11]. Therefore, it is hypothesized that the unique nested-box structure evolved to resist bending forces that occur when the boxfish's dermal armor interlocks and recruits multiple scutes during a biting attack. In other words, the axis of compression during concave bending of the dermal armor would align with the helical axis of the Bouligand structure found in the distal/lateral region and would help explain the unique macro-organization that the boxfish employs in the collagen layer, although further investigation is needed to confirm such a hypothesis. Future research in designing bioinspired Bouligand structures to create novel impact resistant fiber reinforced composites may benefit from learning more about why the boxfish's Bouligand-type structure utilizes the higher-order nested-box structure.

3.3. *In situ scanning electron microscopy*

3.3.1. *Localized failure*

Samples were tested with an *in situ* micro-mechanical testing system to further investigate failure between neighboring scutes and investigate load-bearing capabilities of these structures. Scutes tested in tension (Fig. 7a) showed failure occurring entirely at the interface. The mineralized sutures sustain no visible damage and, while some cracks form within the mineralized plates, the collagen base below can be seen to

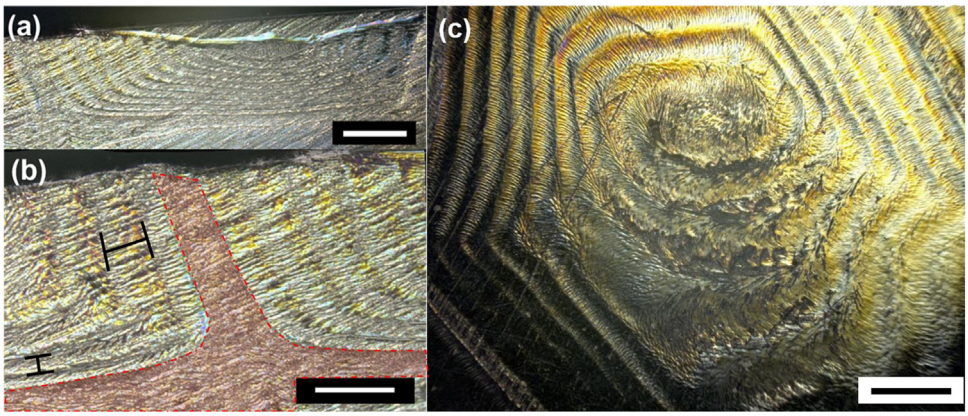

Fig. 5 – Confocal microscopy images of boxfish scute with top mineral plate removed. (a) Cross-section of whole scute revealing the nested-box structure. The pitch length in the distal/lateral regions (100 to 200 μm) is significantly larger than the proximal/central regions (~50 μm). (scale bar, 500 μm); (b) Zoom in on the cross-section of the interface between adjacent scute. The lack of texture to the surface is indicative of a less structured region as compared to inside the scute (scale bar, 200 μm); (c) After careful removal of mineral plate, the periodic collagen structure can be seen. Bottom portion of scute has been damaged through handling (Scale bar, 500 μm).

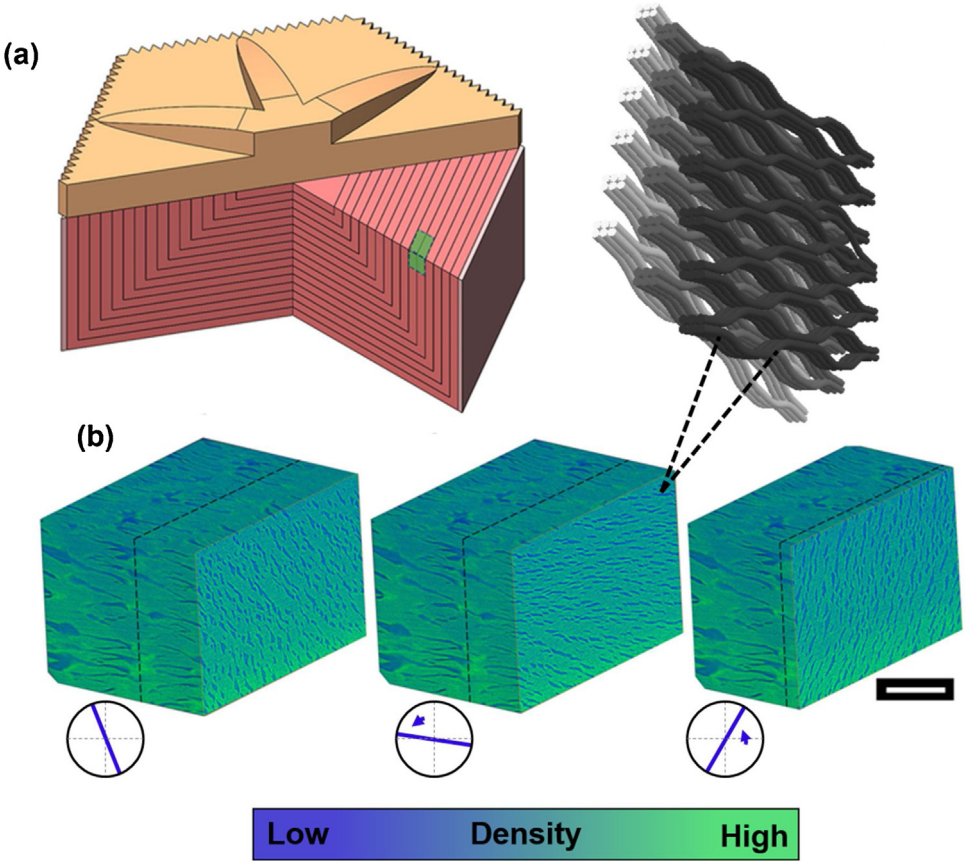

Fig. 6 – (a) Scute model with highlighted region representing approximate location of the micro-computed tomography (μ-CT) 3D images; (b) A series of the same3D μ-CT image is shown where a deeper cross section is taken with each image. The cross sections demonstrate continuous, helical interfibrillar gaps (porosity shown in blue) which are representative of a Bouligand-type structure. The aperture inset is representative of the direction the interfibrillar gaps have rotated to at this given cross-section. The thin, dashed black lines provide a reference between images.3D model of collagen fibrils represents the honeycomb-style Bouligand structure that these data reveal (scale bar, 100 μm).

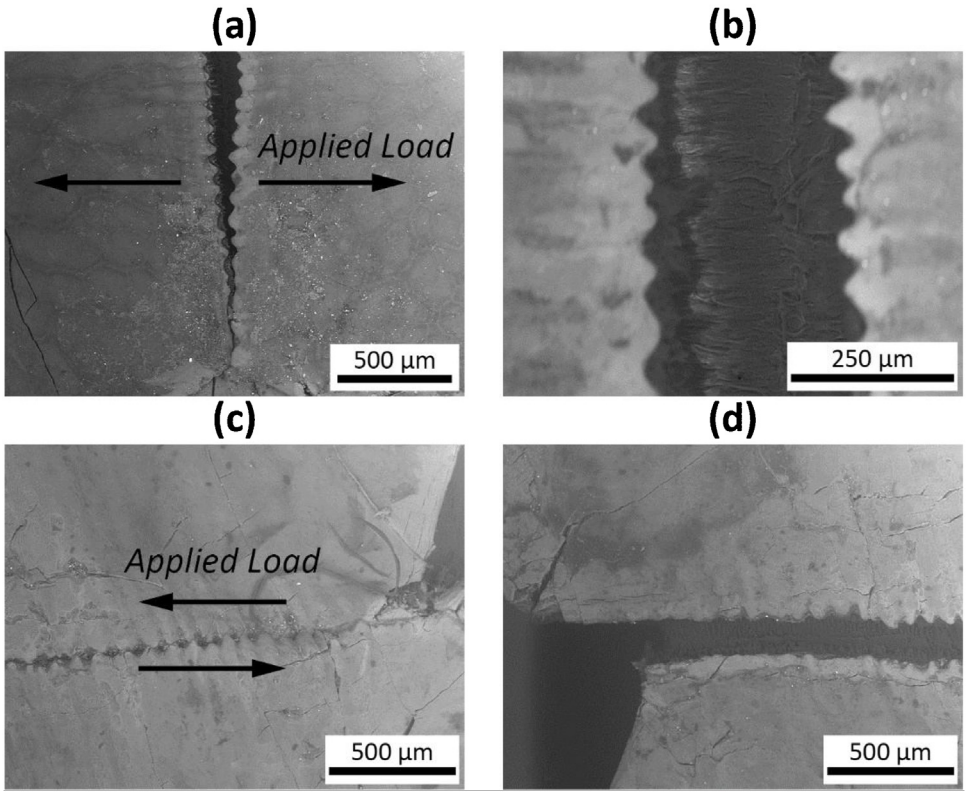

Fig. 7 – *In situ* SEM images with the mineralized plate under: (a, b), tensile loading and (c, d), shear loading. (a) In tension little damage to the mineralized plates is observed with the scutes splitting at the interface; (b) close observation of the interface shows no damage to the mineralized sutures, with the collagen base failing underneath; (c) In shear, the mineralized plate experiences more cracking at and near the sutures; however (d) failure occurs again predominantly in the underlying collagen base.

separate and tear (Fig. 7b). When tested in a shearing mode (Fig. 7c), more damage is visible to the mineralized plate, including the sutures that, in many cases, lock together and fracture. However, final failure still occurs predominantly in the collagen base (Fig. 7d).

Given that the majority of failure occurred in the collagen base which was obscured by the presence of the mineralized plate, *in situ* SEM mechanical testing was performed with the mineralized plate carefully removed. Despite the somewhat weakened structure and the hence exacerbated deformation of the collagen, failure was predominantly located at the interface in both tensile (Fig. 8a) and shearing (Fig. 8b) loading modes. Consistent failure modes both with and without the presence of the mineralized plate suggest that the mineralized plate's primary purpose does not offer significant defense against either tension or shear between the scutes. This is generally consistent with the scales of other fish species, where the outer surface of an individual scale provides a rigid barrier against sharp penetration [7,8], but the combined scale/scute structure provides toughness and ductility [22]. Additionally, the interlocking of the scute's sutured interfaces, unique to the boxfish, during shear modes allows for the force of a predator's attack to efficiently delocalize through the carapace thereby circumventing the issue of lacking enough strength to locally resist the attack [40].

The preferential failure of the scute interfaces may be due to both a gain in flexibility/toughness for the overall dermal armor and to also localize damage on the less structured areas to save in energy costs for self-healing. For the failure to occur preferentially in these interfaces, it is necessary that the interior resist failure and maintain a higher stiffness than the interface. Both the interface and interior are made of the same collagen constituents [4]. Therefore, as is the case of many biological materials [1], the microstructure of the scute's interior must be the source of this increased stiffness.

3.3.2. *Nonlinear deformation response*

When observed in the SEM, the previously observed ladder-like structures of collagen within the scute interior can be seen (Fig. 9a) [4]. However, during *in situ* SEM mechanical loading, it can be seen that these collagen planes deform in a much more complex way than would be expected from a ladder-like structure consisting of bidirectional/orthogonal collagen fibrils; instead, they form a somewhat double-twisted S-shape structure resulting from the applied shear-load (Fig. 9b). This manner of behavior was observed throughout the interior of the scute's collagen base. It is proposed that this structure allows for the collagen planes to distort and realign with an applied stress, providing some measure of isotropy of at least some of its mechanical properties, thereby increasing the deformation resistance of the scute interior, which is similar

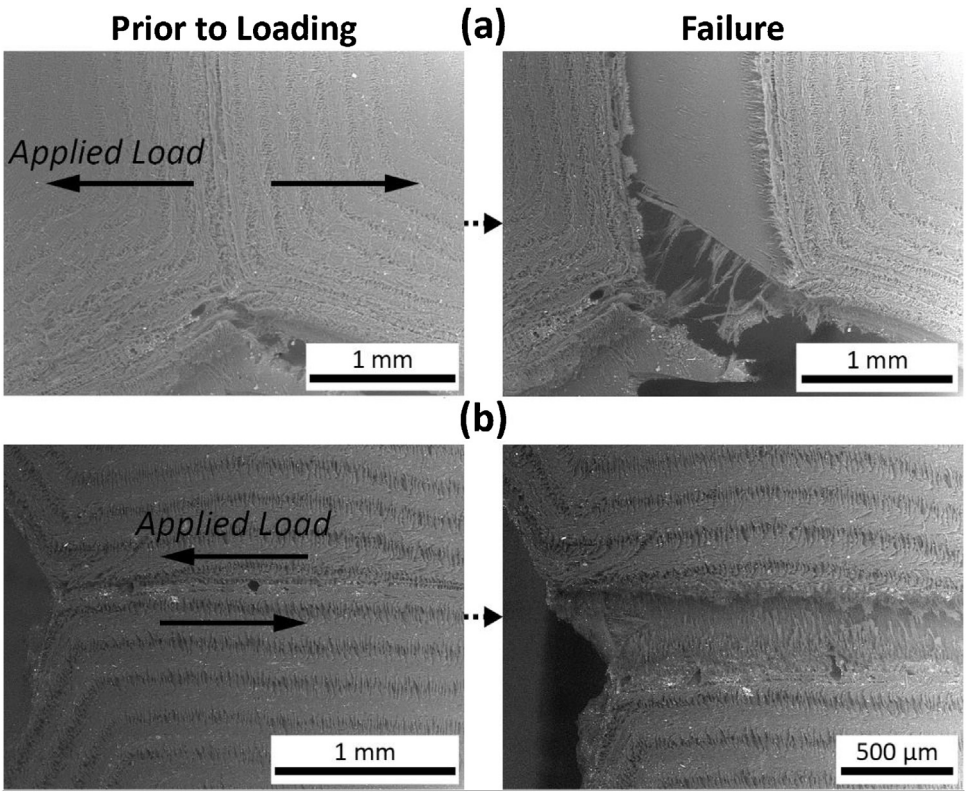

Fig. 8 – *In situ* SEM images with the mineralized plate removed, loaded in (a) tension and (b) shear. Regardless of the loading mode, failure occurs almost entirely at the interface.

to previous conclusions reported for the deformation response of Bouligand structures found in nature [11,18,19].

3.4. *In situ small-angle X-ray scattering*

The SAXS data (Fig. 10a,d) displayed rings superimposed with oriented arcs and broad dot-shaped peaks, which yielded various levels of information that needed to be carefully considered with other data, such as *a priori* knowledge of a Bouligand-type structure and the change in direction of the Bouligand structure throughout the higher-order nested-box structure of the boxfish scute. The dot-shaped peaks derive from the regular spacing of closely packed and closely aligned collagen fibrils; they are similar to patterns reported previously for other natural systems, such as human cornea [36]. Measurements of the distance between neighboring collagen fibrils (roughly the collagen fibril diameter), made from these dots, gave a fibril diameter value of 53 ± 10 nm, which agrees closely with corresponding measurements of collagen fibril diameter in the SEM [4] of 55 ± 10 nm.

Samples were imaged through the thickness of the scutes with different placements of the region of interest (ROI) that helped deduce what attributes were representative of which regions of the underlying nested-box structure (Fig. 10). As shown in Fig. 10a-c, when the ROI is closer to the center of one a scute, a pattern representative of the proximal/central region of the nested-box is observed, where the Bouligand structure is expected to align with the incident x-rays. As shown in Fig. 10d-f, the ROI closer to the interface between the two scutes garnered data that represents both the proximal/central region but also the distal/lateral region, which we hypothesize, from the μ-CT data, is where the Bouligand axis is transverse to the incident x-rays.

Fig. 10a, which targeted the proximal/central region of the nested-box structure, most noticeably demonstrates a unidirectional fibril system from the bold horizontal dots and vertical arcs representative of the periodicities of the lateral packings of collagen fibrils and *d*-period spacing within the fibrils, respectively (Fig. 10b). The direction of these fibrils is orthogonal to the edges of the hexagonal shape of the scute. Additionally, there appears to be a faint concentric ring that suggests the expected Bouligand-structure with its axis parallel to the thickness of the scute and the incident x-rays. Therefore, we corroborate previous results [3] that reveal a combination of both a unidirectional and Bouligand structure network in the proximal/central region.

Fig. 10d, which encapsulates both regions of the nested-box structure, contains nearly identical information to Fig. 10a but also appears to include an orthogonal direction of unidirectional fibrils. However, due to previous reports on the presence of a Bouligand structure [3] and the findings in this work with μ-CT, we hypothesize that these attributes are likely due to the SAXS beam interacting with the Bouligand structure transverse to its helical axis rather than due to additional unidirectional fibrils. It is worth noting that Besseau and Bouligand [3] also found unidirectional fibrils running transverse (aligned with the thickness of the scute) to the Bouligand structure in the distal/lateral region. However, we

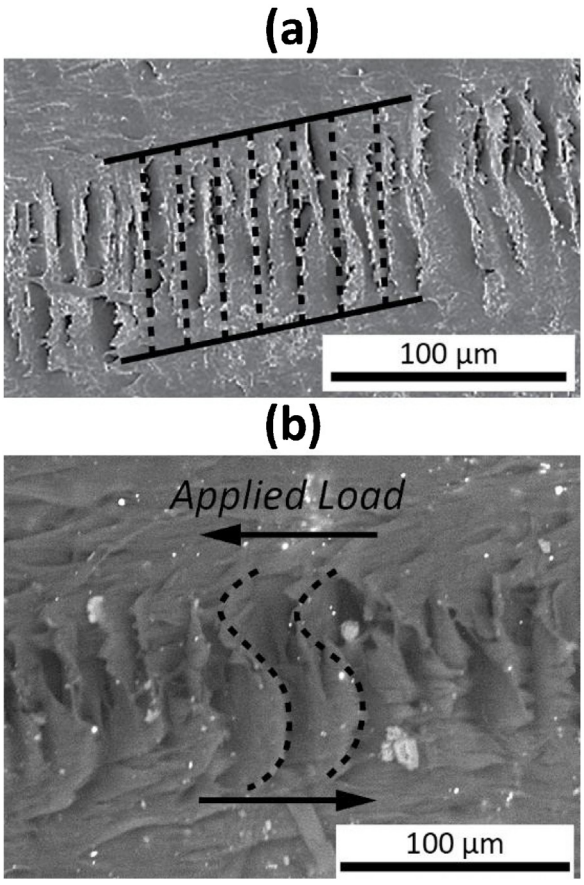

Fig. 9 – (a) The ladder-like structures within the interior of the scute's collagen base consist of collagen planes (dashed lines) that bridge the gap between dense collagen bands (solid lines); (b) When a shearing load is applied to this structure, the collagen planes deform into a complex, sinusoidal shape.

do not expect these fibrils to contribute much to the resultant diffraction patterns as the fibrils are aligned with the incident x-rays and, therefore, their *d*-periods are effectively hidden.

Overall, we observed three main characteristics resulting from the SAXS patterns, utilizing previous research on the boxfish collagen structure, evidence from data acquired in this work, and the fundamental knowledge of the interaction of SAXS in collagen systems. These three main characteristics, shown in Fig. 11 are:

- A Bouligand structure in the proximal/central region of nested-box structure.
- A unidirectional network of radial collagen fibrils that transversely intersect the Bouligand structure in the proximal/central region.
- A Bouligand structure in the outer/top region with its helical axis transverse to the thickness of the scute and aligned normal to the hexagonal edges of the scute.

When mechanically tested *in situ*, the scutes showed surprising ductility, especially in shear (Fig. 12). The stiffness during tensile tests is likely due to the alignment of the unidirectional collagen fibrils in the proximal/central region of the scutes with the tensile axis. Conversely, the ductility observed in shear tests is likely due the non-linear deformation responses previously observed with *in situ* SEM. The dotted lines in Fig. 12c,d represent a theoretical maximum where all tissue strains are due to the tensile deformation of the constituent collagen fibrils. The data demonstrate a considerable portion of the tissue strain is not from the fibrils being tracked through SAXS. This is expected, as the collagen in the scute is organized into a complex network that cannot be simply explained through the fibril strains of only the underlying unidirectional system. Moreover, in Fig. 12d, a tissue strain of over 40% is observed, while only reaching a fibril strain of ~3%. This corroborates the hypothesis that the system of collagen being observed in the SAXS diffraction patterns is normal to the hexagonal edges of the scutes; therefore, they are perpendicular to the shearing axis explaining why modest fibril tensile strain is observed.

3.5. *Finite element modeling of bouligand structure in shear*

To understand the reason why the S-shape developed in collagen after a shear test, a 3D finite element (FE) model of material element cell was developed by an arrangement of N ($N = 20$) stacked layers of continuum shell elements of thickness l and a pitch distance of L as presented in Fig. 13a. This material element cell represents the behavior of the Bouligand structure inside the collagen scutes, showing the material element cell in the forms of N helicoidally stacked layers with different orientations. The unit cell contains layers of linear elastic layers with the pitch angle of 9°.The orthotropic elastic properties that are used for this study are the following [41]:

$$E_1 = 144\,GPa,\ \nu_{12} = 0.44, G_{12} = 47.2\,GPa$$

$$E_2 = 76\,GPa,\ \nu_{13} = 0.06,\ G_{13} = 25.6\,GPa$$

$$E_3 = 82\,GPa,\ \nu_{23} = 0.18,\ G_{23} = 41.3\,GPa$$

The layers are completely bonded together, and shear displacement-controlled load is applied to the top and bottom surface of the model. The horizontal displacement (u_x) of the Bouligand unit cell under shear loading is presented in Fig. 13b. The comparison between normalized horizontal displacement of both a homogenized material and the Bouligand microstructure are presented in Fig. 13c. Results present a S-shape response for the Bouligand unit cell although the material assigned to the layers is linear elastic. This nonuniform displacement distribution can be related to the Bouligand orientation of the unit cell and thus, one can conclude that the Bouligand orientation inside the unit cell induces a non-homogeneous displacement across an entire pitch.

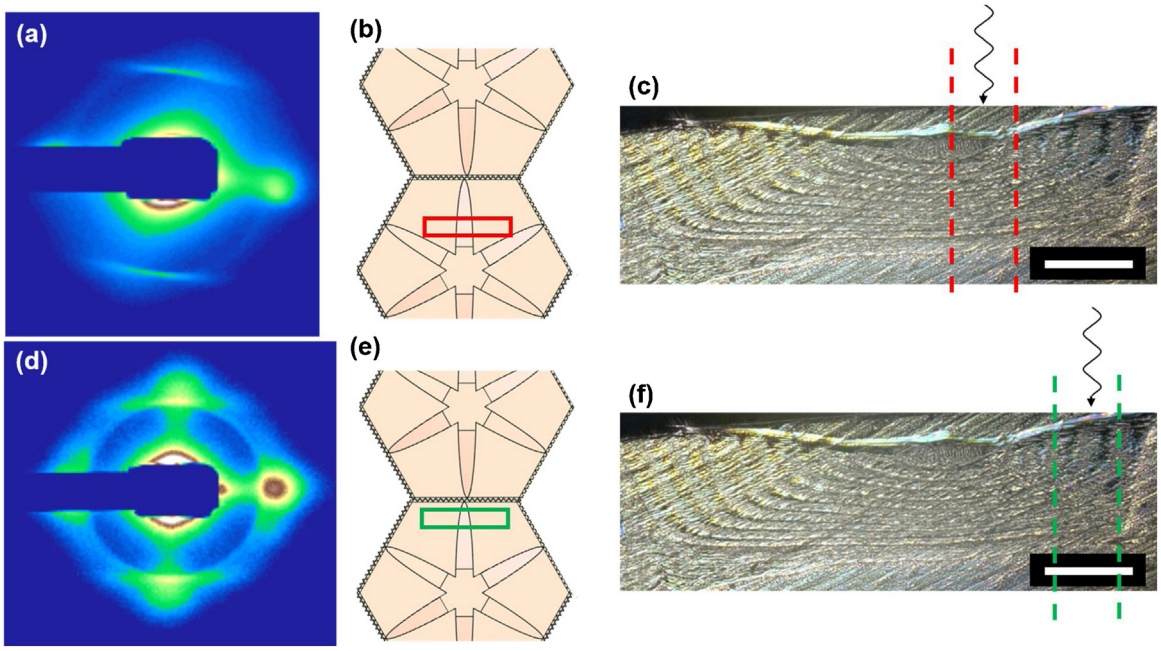

Fig. 10 – (a, d) Small angle x-ray scattering diffraction (SAXS) patterns from boxfish scutes. (b, e) Representation of two neighbored boxfish scutes anchored vertically to apply a tensile load. Red and green rectangles represent the regions of interest (ROI); (c, f) Confocal microscopy cross-section view of nested-box collagen structure. Dotted lines represent the width of ROI to reveal which sections of the structure were analyzed with SAXS. (scale bar: 0.5 mm) (a) Displays a pair of vertical arcs and horizontal dots that represent the *d*-period of collagen and the lateral packing of collagen fibrils, respectively. (d) Displays two pairs of dots and arcs orthogonal to each other which is proposed to be representative of both the proximal/central region and distal/lateral regions.

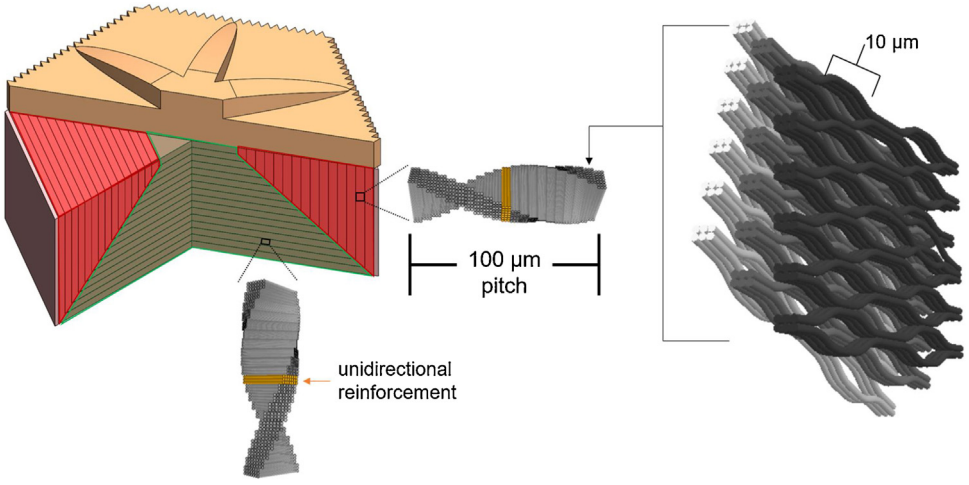

Fig. 11 – Summary of structural characterizations within the collagen beneath a scute. The scute is comprised of a hexagonal nested-box structure that contains rotating lamellae of collagen fibrils that either have its axis of rotation (Bouligand axis) parallel or transverse to the thickness of the scute. The Bouligand structures parallel to thickness dominate the inner and lower regions (green) of the scute, whereas the Bouligand structure transverse dominate the top and outer regions (red), giving rise to the overall nested-box appearance. These Bouligand structures in both regions are reinforced by a separate unidirectional network of collagen fibrils that run transverse the Bouligand axis. μ-CT revealed that the distal/lateral regions contained spiraling interfibrillar gaps that are like those found the exoskeleton of the lobster *Homarus americanus* and exocuticle of the weevil *Curculio longinasus* [36–38].

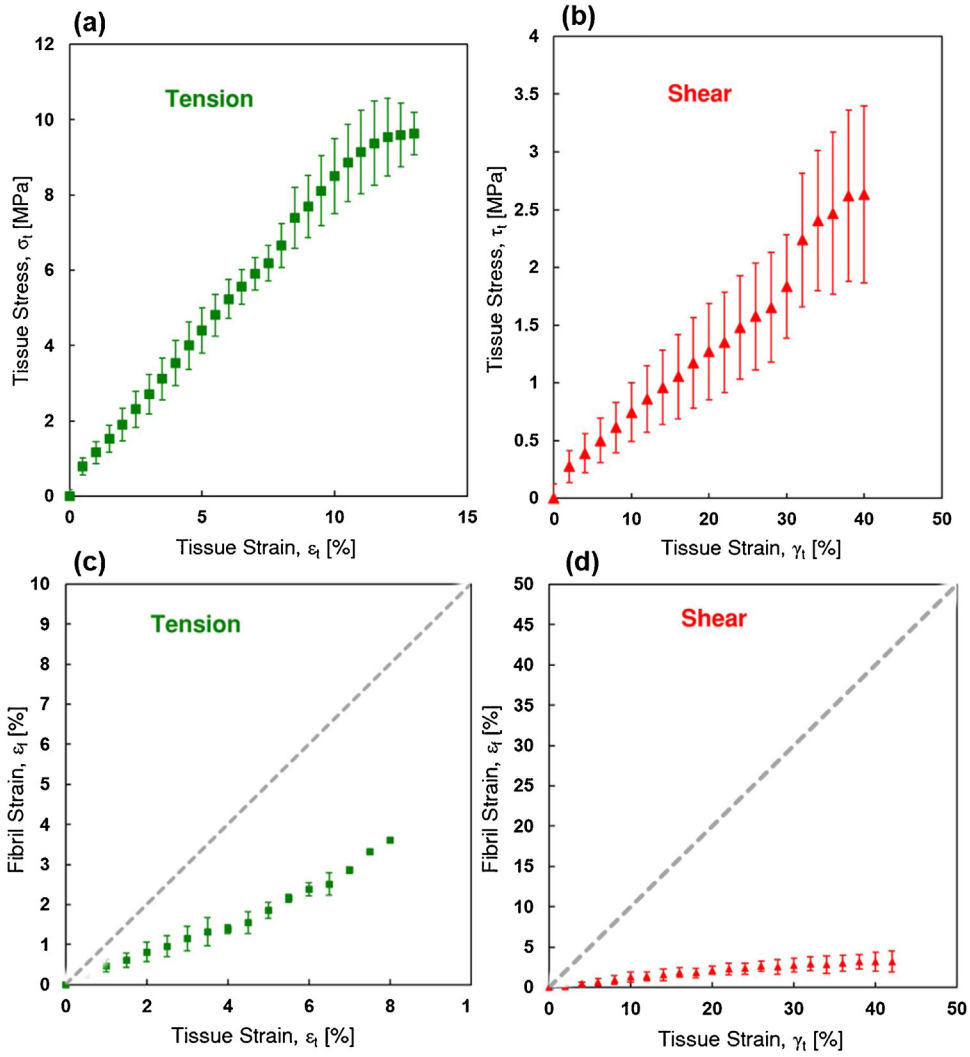

Fig. 12 – Mechanical data produced from *in situ* small-angle x-ray scattering (SAXS) on neighboring scutes with their mineral plates removed; (a),(c) and (b),(d) are the averaged data from the tensile and shear experiments, respectively. Tissue strain was obtained using digital image correlation to track the relative movements of the surface texture of the collagen network. Fibril strains were taken from the *d*-period arcs produced from the unidirectional fibrils in the proximal/central regions of the scutes. Dotted lines represent a 1:1 relationship between the tissue and fibril strains that would be produced if all strain occurring on the tissue level was due to the stretching or compressing of the constituent collagen fibrils; Results demonstrate the scutes are designed to be stiffer and stronger in a tensile mode, while more ductile in a shear mode.

3.6. *Finite element modeling of collagen interface between scutes*

3.6.1. *Collagen scute geometry*

FE models of the collagen scutes without mineralized plates (similar to those examined in the *in situ* SEM tests) were developed to characterize both the collagen and its interface connection. Testing a single coupon sample of scutes was too difficult due to their small size; as a result, the *in situ* SEM tensile experiments were performed between two scutes without mineralized plates. Such *in situ* SEM tests generated a variety of stress-strain curves. The upper and lower load-displacement curves from experimental tests are termed as the upper and lower bounds, respectively. The dimensions of the scutes related to the upper and lower bounds are presented in Table 1. In the modeling, the effect of the Bouligand microstructure was ignored inside the collagen and an interface between the hexagonal collagen base was modeled with zero thickness cohesive elements, as shown in Fig. 14a.

Table 1 – The initial geometry of the collagen scutes used for the tensile test.

Test numbers	Average width (mm)	Average thickness (mm)	Initial length L_0 (mm)
Lower bound	3.76	0.54	2.68
Upper bound	3.38	0.64	2.94

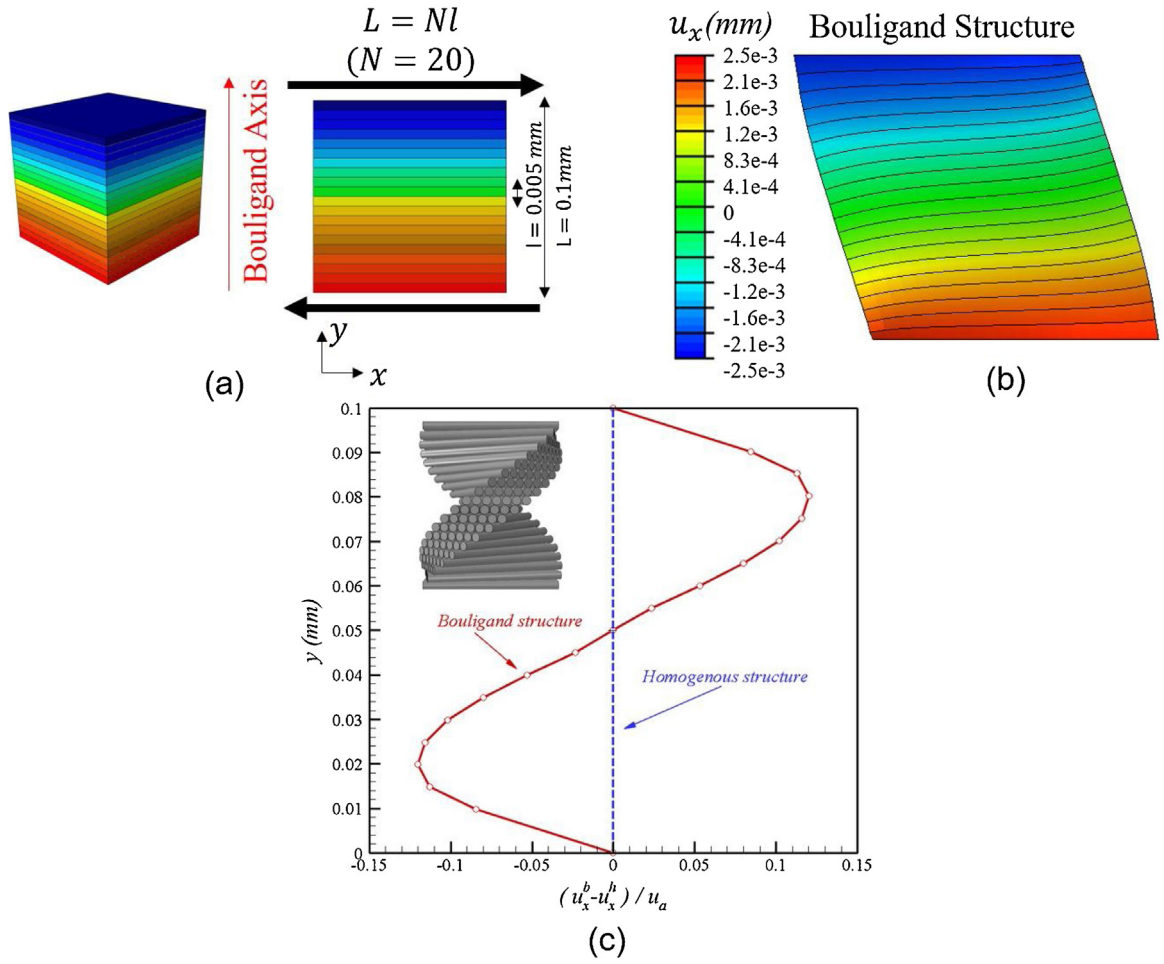

Fig. 13 – (a) Schematic diagram of the layered model for finite element modeling studies. The parameter, *L* is the pitch distance (the distance to make a rotation of 180°); *l* is the layer thickness; *N* is the number of layers in the pitch and is equal to 20, (b) horizontal displacement of element unit cell for Bouligand cells, (c) the normalized horizontal displacements of Bouligand structure and homogenous material along vertical (*y*) direction.

3.6.2. *Type I collagen and interface characterization*

The mechanical properties of pure collagen are not available in the literature. Previous studies on collagen of different species do not necessarily represent collagen materials that are pertinent to boxfish scutes, but instead present a wide spectrum of collagen with varying fibril densities and orientations [42–47]. Type I collagen is found in body of many animals in nature; for example, rat tail, rabbit skin, human skin, human tendons, bone [42–47]. In all the cases, the collagen has shown a hyperelastic behavior. Thereby, in this section a parametric and systematic study was run to develop the stress-strain curves for collagen in boxfish scute using the experimental data from our *in situ* SEM tensile tests. Since the *in situ* test was not a pure uniaxial test, the stress-strain curve for collagen cannot be obtained directly. As such, several FE analyses were needed to fit the correct behavior of both the collagen and interface. The process of separation between two scutes under tensile loading, based on SEM observation [4], confirmed that separation between two scutes occurs along the interface between two scutes in the underlying collagen base.

The initial stiffnesses from the stress-strain curves in the *in situ* experiments are related to the hexagonal collagen base material while, the interface is mainly responsible for the values of peak stress and failure strain obtained from the stress-strain curves. Several FE simulations with various hyperelastic ranges, including the geometry of the upper and lower bounds, were developed to estimate the initial stiffness of the collagen base. In the FE models, once the correct initial stiffness of the collagen was determined, the next step was to develop an accurate model for the cohesive interface. The bilinear separation law in ABAQUS [48] can be defined by two parameters, the maximum normal strength (σ_{max}), and fracture energy (G_{IC}).

To validate the uniqueness of the result for the cohesive interface, two sets of parametric analyses were conducted. For the first case study, the maximum strength was kept constant, and the fracture energy was changed, while for the second case study, the fracture energy was kept constant, and the value of maximum stress was varied. The results were found to produce a good match of the simulations and these parametric studies and are presented in Table 2 and Fig. 14.

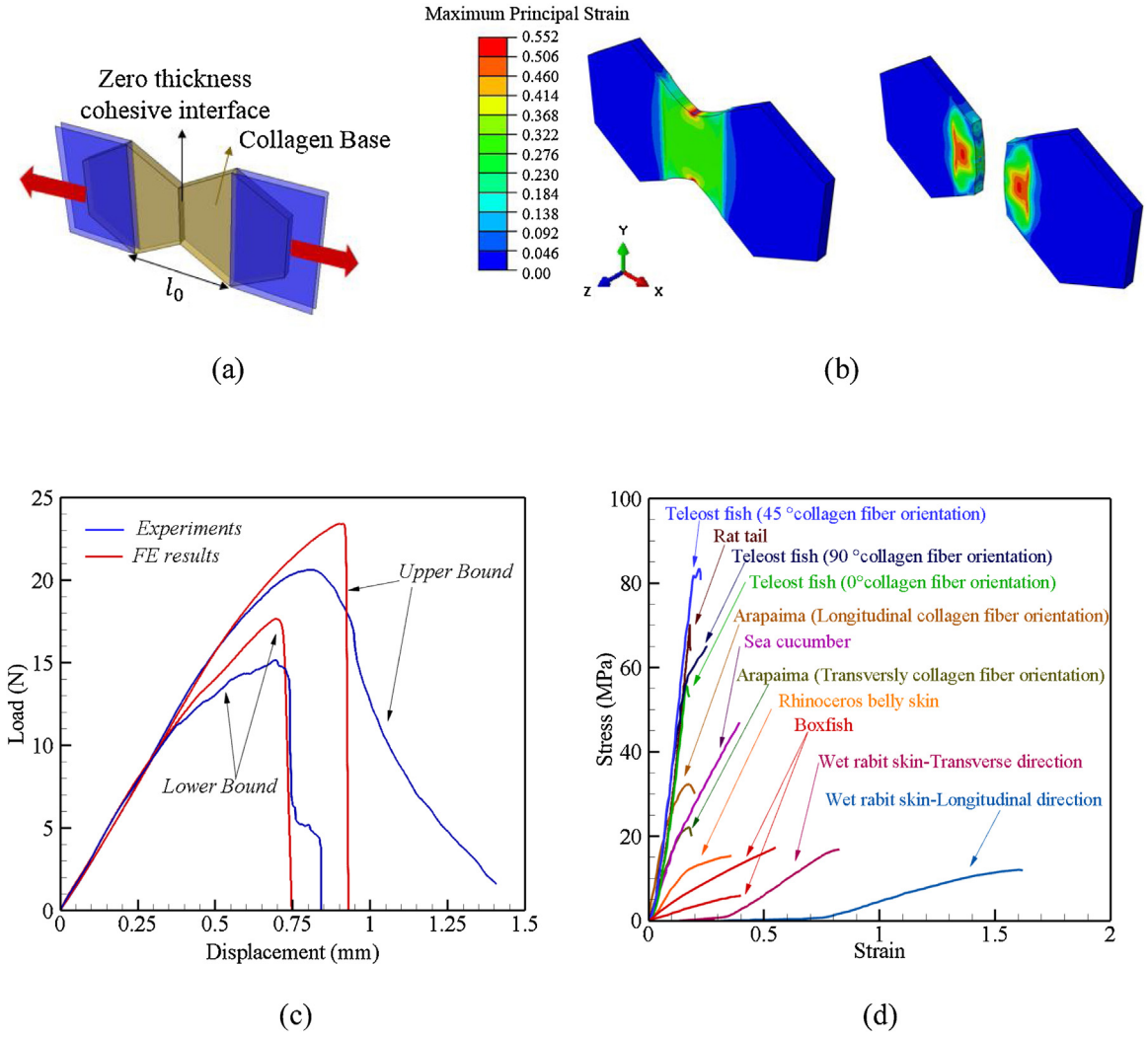

Fig. 14 – FE model for two collagen scute, (a) boundary condition and geometry of the two collagen along with the zero thickness cohesive interface, (b) the maximum principal strain distribution along two collagen scute under tensile loading in the middle of loading and after separation, (c) a comparison between the load-displacement curves from the FE models for the upper and lower bounds and SEM tests of two collagen scute, (d) a comparison between the stress-strain curve of collagen in boxfish and various animal in nature [42–47].

Table 2 – Cohesive interface characterization using ABAQUS for the lower and upper bounds.

	Maximum normal strength σ_{max} (MPa)	Fracture energy G_{IC}
Lower bound	12	5
Upper bound	15	8

3.6.3. *Finite element results and discussion*

The Lagrangian strain contour of the FE model for two-collagen bases during tensile loading and after separation is presented in Fig. 14b. The FE results state that the strain concentration occurs along the interface area. A comparison between the finite element model and SEM tensile tests of two collagen scutes without the mineralized plate is presented in Fig. 14c. The displacement-controlled load was applied on the boundary condition for the FE models. As the displacement increases in the boundaries, the value of reaction force increases up to the peak load. The comparison between FE simulation and experiments confirmed similar initial stiffness for both upper and lower bounds. As previously discussed, the nominal strength of the interface is responsible for the peak load in the force-displacement curve. After reaching the peak load, the interface starts stretching until the separation occurs between two hexagonal collagen scutes. In the modeling, the cohesive elements of the interface are removed as they reach the final fracture energy and a complete separation can be observed in simulations after all the cohesive elements were removed (Fig. 14b). For the purpose of comparison, the stress-strain curves of type I collagen of various animals with the type I collagen in boxfish (results from the characterization) are presented in Fig. 14d [42–47]. These curves offer enormous variety in the stress-strain curves of collagen because the collagen fibril's hierarchical organization varies among different species and tissues. Finally, there is excellent agreement between the

load-displacement curves for simulation and experimental results.

4. Conclusions

While other fish species ensure flexibility of both their armor and bodies through overlapping scales, the rigid-bodied boxfish utilizes unique adaptations to delocalize compressive stress from predator bites, thereby providing itself a higher level of defense than its counterparts. The results described here point to numerous mechanisms that the boxfish employs to ensure its defense. Confocal microscopy and micro-computed tomography (μ-CT) revealed that underneath the mineralized plate is a complex system of collagen fibrils in a Bouligand-type structure organized into a higher-order nested-box structure. As observed through *in situ* scanning electron microscopy (SEM) mechanical testing and confirmed through finite element analysis, the Bouligand structure will deform and align with loading, allowing for some manner of mechanical property isotropy. *In situ* small-angle x-ray scattering further reveals the complex network of collagen and shows how individual collagen fibrils get stretched and compressed to accommodate the whole-scute's change of shape and deformation. This complex organization of stretched/compressed fibrils allows for relatively large levels of tissue strain to occur without inducing scute fracture, providing enhanced ductility and toughness. Furthermore, the collagen interface between scutes is less dense and complex in structure than the organized interior of the scute. In addition, the mineralized sutures account for only ~4% of the thickness of the interface and provide little or no mechanical advantage there. Failure both with the mineralized plate and without occurs at the interface with little or no damage to the scute interior. All of this results in a structure that ensures failure occurs predominantly at the interface between scutes where greater flexibility can be achieved while maintaining the complex interior of the scute intact.

Based upon this study's results on the structure and *in-situ* failure mechanisms of the boxfish's rigid armor, the following conclusions can be made:

- The boxfish employs a novel Bouligand-type structure (nested-box) that employs abrupt 90° shifts in its orientation that is unlike any other Bouligand-type structures found in nature.
- A rare analog of the Bouligand-structure is observed in the distal/lateral regions referred to as a honeycomb structure previously seen in the exoskeleton of the *Homaris americanus* lobster and the exocuticle of the *Curculio longinasus* weevil.
- The interfaces of the boxfish's scutes are less dense and complex than the interior and feature very little mechanical reinforcement from the mineralized surface plate and interlocking sutures. This structure provides flexibility at the interface and ensures that failure occurs at specific locations when mechanically stressed in tension or shear. The combination of a compliant interface and stiff interior to the boxfish's scutes allows for it to maintain some flexibility for both motion and defense despite its rigid and non-overlapping armor.
- The interior of the boxfish's scutes consist of a complex collagen-based structure that combines a unidirectional network of collagen fibrils intersecting with Bouligand-type structures. When mechanically stressed, these structures are capable of deforming to align with the applied force and provide damage resistance. These adaptations allow for the interior of the boxfish's scutes to resist damage and provide defense.
- The 3D finite element results of the unit cell with the Bouligand microstructure confirm the S-shape shear deformation response seen in experimental results with *in situ* SEM and suggest this unique response is due to the Bouligand orientation of the unit cell.

Further studies on the complex and novel collagen structure of the boxfish will aid in the field of bioinspired fiber reinforced materials, and more specifically in understanding the different tropes and utility of a Bouligand, or twisted plywood, structure. These novelties that are worth further exploration for use in lightweight reinforced materials are the following:

1 Utilization of abrupt 90° changes in the orientation of Bouligand structures, overall referred to as the nested-box structure. We hypothesize this is used in response to converting compressive biting forces into a delocalized concave bending that both interlocks the mineral scutes and also applies in-plane compressive forces which align with the distal/lateral Bouligand axis. Exploring the nested-box Bouligand structure under bending may further elaborate on the utility of this novel structure.
2 Employing the honey-comb structure, also seen in the lobster *Homarus americanus* and the weevil *Curculio longinasus* [37–39]. This structure is previously proposed to both supply microchannels for nutrients supply and also to provide a high density of interfaces to avoid fiber pullout. Exploring bio-inspired fiber composites that can utilize the channels of a honey-comb derivative of a Bouligand structure for transport of a self-healing matrix or to help tune the bulk density are likely worth exploring.
3 The boxfish applies a combination of Bouligand structures with unidirectional fibrous networks of collagen, and further exploring this strategy may reveal how to further control the mechanical properties of Bouligand structures in specified directions under various loading conditions.

Conflict of interest

The authors declare no conflicts of interest.

Acknowledgements

This work is supported by a Multi-University Research Initiative through the Air Force Office of Scientific Research (AFOSR-FA9550-15-1-0009). We thank the A.Z. Weber group for providing their tensile stage, which was supported by DOE EERE Fuel-Cell Performance and Durability Consortium (FC-PAD). This work was performed in part at the San Diego Nanotechnology Infrastructure (SDNI) of UCSD, a member

of the National Nanotechnology Coordinated Infrastructure, which is supported by the National Science Foundation (Grant ECCS-1542148). This work used the Extreme Science and Engineering Discovery Environment (XSEDE), which is supported by National Science Foundation grant number ACI-1548562 [[49]]. We also acknowledge the use of beamline 7.3.3 at the Advanced Light Source, which is supported by the U.S. Department of Energy, Office of Science, Office of Basic Energy Sciences, Division of Materials Sciences and Engineering, under contract no. DE-AC02-05CH11231 to the Lawrence Berkeley National Laboratory. Special thanks are due to Prof. P. Hastings of the Scripps Institute of Oceanography, UC San Diego, for providing the boxfish specimens and Dr. James Tyler of the Smithsonian for helpful discussions.

REFERENCES

[1] Naleway SE, Porter MM, McKittrick J, Meyers MA. Structural design elements in biological materials: application to bioinspiration. Adv Mater 2015;27:5455–76.
[2] Meunier FJ, Francillon Viellot H. Structure and mineralization of the scutes in ostracion lentiginosum (Teleostei, tetraodontiforme, ostraciidae). Annales des Sciences Naturelles-Zoologie et Biologie Animale 1995;16:33–46.
[3] Besseau L, Bouligand Y. The twisted collagen network of the box-fish scutes. Tissue Cell 1998;30:251–60.
[4] Yang W, Naleway SE, Porter MM, Meyers MA, McKittrick J. The armored carapace of the boxfish. Acta Biomater 2015;23:1–10.
[5] Naleway SE, Taylor JRA, Porter MM, Meyers MA, McKittrick J. Structure and mechanical properties of selected protective systems in marine organisms. Mater Sci Eng C 2016;59:1143–67.
[6] Yang W, Chen IH, Gludovatz B, Zimmermann EA, Ritchie RO, Meyers MA. Natural flexible dermal armor. Adv Mater 2013;25:31–48.
[7] Zhu D, Ortega CF, Motamedi R, Szewciw L, Vernerey F, Barthelat F. Structure and mechanical performance of a "modern" fish scale. Adv Eng Mater 2012;14:B185–94.
[8] Zhu DJ, Szewciw L, Vernerey F, Barthelat F. Puncture resistance of the scaled skin from striped bass: collective mechanisms and inspiration for new flexible armor designs. J Mech Behav Biomed Mater 2013;24:30–40.
[9] Bruet BJF, Song JH, Boyce MC, Ortiz C. Materials design principles of ancient fish armour. Nat Mater 2008;7:748–56.
[10] Song JH, Ortiz C, Boyce MC. Threat-protection mechanics of an armored fish. J Mech Behav Biomed Mater 2011;4:699–712.
[11] Yang W, Sherman VR, Gludovatz B, Mackey M, Zimmermann EA, Chang EH, et al. Protective role of Arapaima gigas fish scales: structure and mechanical behavior. Acta Biomater 2014;10:3599–614.
[12] Yang W, Gludovatz B, Zimmermann EA, Bale HA, Ritchie RO, Meyers MA. Structure and fracture resistance of alligator gar (Atractosteus spatula) armored fish scales. Acta Biomater 2013;9:5876–89.
[13] Zimmermann EA, Gludovatz B, Schaible E, Dave NKN, Yang W, Meyers MA, et al. Mechanical adaptability of the Bouligand-type structure in natural dermal armour. Nat Commun 2013;4:2634.
[14] Bouligand Y. Twisted fiberous arrangements in biological materials and cholesteric mesophases. Tissue Cell 1972;4:189–217.
[15] Dastjerdi AK, Barthelat F. Teleost fish scales amongst the toughest collagenous materials. J Mech Behav Biomed Mater 2015;52:95–107.
[16] Sharma V, Crne M, Park JO, Srinivasarao M. Bouligand structures underlie circularly polarized iridescence of scarab beetles: a closer view. Mater Today Proc 2014;1:161–71.
[17] Yang R, Zaheri A, Gao W, Hayashi C, Espinosa HD. Exoskeletons: AFM identification of beetle exocuticle: Bouligand structure and nanofiber anisotropic elastic properties. Adv Funct Mater 2017;27(6).
[18] Yaraghi NA, Guarín-Zapata N, Grunenfelder LK, Hintsala E, Bhowmick S, Hiller JM, et al. Biocomposites: a sinusoidally architected helicoidal biocomposite. Adv Mater 2016;28(32), 6769-6769.
[19] Suksangpanya N, Yaraghi NA, Kisailus D, Zavattieri P. Twisting cracks in Bouligand structures. J Mech Behav Biomed Mater 2017;76:38–57.
[20] Vernerey FJ, Barthelat F. Skin and scales of teleost fish: simple structure but high performance and multiple functions. J Mech Phys Solids 2014;68:66–76.
[21] Vernerey FJ, Barthelat F. On the mechanics of fishscale structures. Int J Solids Struct 2010;47:2268–75.
[22] Vernerey FJ, Musiket K, Barthelat F. Mechanics of fish skin: a computational approach for bio-inspired flexible composites. Int J Solids Struct 2014;51:274–83.
[23] Lin YS, Wei CT, Olevsky EA, Meyers MA. Mechanical properties and the laminate structure of Arapaima gigas scales. J Mech Behav Biomed Mater 2011;4:1145–56.
[24] Wang B, Yang W, Sherman VR, Meyers MA. Pangolin armor: overlapping, structure, and mechanical properties of the keratinous scales. Acta Biomater 2016;41:60–74.
[25] Connors MJ, Ehrlich H, Hog M, Godeffroy C, Araya S, Kallai I, et al. Three-dimensional structure of the shell plate assembly of the chiton *Tonicella marmorea* and its biomechanical consequences. J Struct Biol 2012;177:314.
[26] Martini R, Barthelat F. Stretch-and-release fabrication, testing and optimization of a flexible ceramic armor inspired from fish scales. Bioinspir Biomim 2016;11:066001.
[27] Li Y, Ortiz C, Boyce MC. A generalized mechanical model for suture interfaces of arbitrary geometry. J Mech Phys Solids 2013;61:1144–67.
[28] Li Y, Ortiz C, Boyce MC. Stiffness and strength of suture joints in nature. Phys Rev E 2011;84:062904.
[29] Li Y, Ortiz C, Boyce MC. Bioinspired, mechanical, deterministic fractal model for hierarchical suture joints. Phys Rev E 2012;85:031901.
[30] Feilden E, Ferraro C, Zhang Q, García-Tuñón E, D'Elia E, Giuliani F, et al. 3D printing bioinspired ceramic composites. Sci Rep 2017;7(1).
[31] Natarajan B, Krishnamurthy A, Qin X, Emiroglu CD, Forster A, Foster EJ, et al. Binary cellulose nanocrystal blends for bioinspired damage tolerant photonic films. Adv Funct Mater 2018;28(26):1800032.
[32] Nguyen T, Peres BU, Carvalho RM, Maclachlan MJ. Photonic hydrogels from chiral nematic mesoporous chitosan nanofibril assemblies. Adv Funct Mater 2016;26(17):2875–81.
[33] Hastings PA, Walker HJ, Galland GR. Fishes: a guide to their diversity. Berkeley: University of California Press; 2015.
[34] Hexemer A, Bras W, Glossinger J, Schaible E, Gann E, Kirian R, et al. A SAXS/WAXS/GISAXS beamline with multilayer monochromator. J Phys Conf Ser 2010;247:012007.
[35] Barth HD, Zimmermann EA, Schaible E, Tang SY, Alliston T, Ritchie RO. Characterization of the effects of x-ray irradiation on the hierarchical structure and mechanical properties of human cortical bone. Biomaterials 2011;32(34):8892–904.
[36] Meek KM, Quantock AJ. The use of x-ray scattering techniques to determine corneal ultrastructure. Prog Retin Eye Res 2001;20(1):95–137.
[37] Raabe D, Romano P, Sachs C, Al-Sawalmih A, Brokmeier H, Yi S, et al. Discovery of a honeycomb structure in the twisted

plywood patterns of fibrous biological nanocomposite tissue. J Cryst Growth 2005;283(1-2):1–7.
[38] Romano P, Fabritius H, Raabe D. The exoskeleton of the lobster Homarus americanus as an example of a smart anisotropic biological material. Acta Biomater 2007;3(3):301–9.
[39] Jansen MA, Singh SS, Chawla N, Franz NM. A multilayer micromechanical model of the cuticle of Curculio longinasus Chittenden, 1927 (Coleoptera: curculionidae). J Struct Biol 2016;195(2):139–58.
[40] Chintapalli RK, Mirkhalaf M, Dastjerdi AK, Barthelat F. Fabrication, testing and modeling of a new flexible armor inspired from natural fish scales and osteoderms. Bioinspir Biomim 2014;9(3):036005.
[41] Barthelat F, Li CM, Comi C, Espinosa HD. Mechanical properties of nacre constituents and their impact on mechanical performance. J Mater Res 2006;21(8):1977–86.
[42] Gentleman E, Lay AN, Dickerson DA, Nauman EA, Livesay GA, Dee KC. Mechanical characterization of collagen fibers and scaffolds for tissue engineering. Biomaterials 2003;24(21):3805–13.
[43] Haut RC. The influence of specimen length on the tensile failure properties of tendon collagen. J Biomech 1986;19(11):951–5.
[44] Miyazaki H, Kozaburo H. Tensile tests of collagen fibers obtained from the rabbit patellar tendon. Biomed Microdevices 1999;2(2):151–7.
[45] Tingting Yang, Wang Wen, Zhang Hongze, Li Xinming, Shi Jidong, He Yijia, Zheng Quan-shui, Li Zhihong, Zhu Hongwei. Tactile sensing system based on arrays of graphene woven microfabrics: electromechanical behavior and electronic skin application. ACS Nano 2015;9(11):10867–75.
[46] Rigby Bernard J, Hirai Nishio, Spikes John D, Eyring Henry. The mechanical properties of rat tail tendon. J Gen Physiol 1959;43(2):265–83.
[47] Freed AD, Doehring TC. Elastic model for crimped collagen fibrils. J Biomech Eng 2005;127(4):587–93.
[48] ABAQUS 2018 Abaqus Analysis User's Manual (RI, USA: SIMULIA Inc).
[49] Towns John, Cockerill Timothy, Dahan Maytal, Foster Ian, Gaither Kelly, Grimshaw Andrew, et al. XSEDE: accelerating scientific discovery. Comput Sci Eng 2014;16(5 (Sept.-Oct)):62–74, http://dx.doi.org/10.1109/MCSE.2014.80.